

**Prediction of the two-dimensional cobalt carbonitride compounds  $\text{CoN}_4\text{C}_{10}$ ,  $\text{Co}_2\text{N}_8\text{C}_6$ , and  $\text{Co}_2\text{N}_6\text{C}_6$** Dapeng Liu,<sup>1</sup> Shuo Zhang,<sup>1</sup> Miao Gao,<sup>2</sup> and Xun-Wang Yan<sup>1,\*</sup><sup>1</sup>*College of Physics and Engineering, Qufu Normal University, Qufu, Shandong 273165, China*<sup>2</sup>*Department of Physics, School of Physical Science and Technology, Ningbo University, Zhejiang 315211, China*

(Received 22 July 2020; revised 1 December 2020; accepted 10 February 2021; published 4 March 2021)

Single-atom-thick two-dimensional material containing 3d transition metal was rarely reported in the past. Based on the first principles method, we predict that the cobalt carbonitrides  $\text{CoN}_4\text{C}_{10}$ ,  $\text{Co}_2\text{N}_8\text{C}_6$ , and  $\text{Co}_2\text{N}_6\text{C}_6$  are a new class of two-dimensional (2D) materials, which are made up of two components: the  $\text{CoN}_4$  unit and the graphene fragment unit, arranged in a planar pattern. The stability of the  $\text{CoN}_4\text{C}_{10}$ ,  $\text{Co}_2\text{N}_8\text{C}_6$ , and  $\text{Co}_2\text{N}_6\text{C}_6$  monolayers is demonstrated by the formation energy and phonon spectra calculations, as well as the molecular dynamics simulations. The spin-polarized calculations reveal that all three compounds are magnetic metals, and the electronic states near Fermi energy are dominated by Co 3d electronic states. Moreover, there exist a few sharp peaks of density of state in the vicinity of Fermi energy, deriving from the  $d_{z^2}$  orbitals of Co atom. Thus, the graphenelike transition-metal carbonitrides are not only a new class of 2D materials with single-atom-thickness but also have rich electronic properties due to the incorporation of transition metal.

DOI: [10.1103/PhysRevB.103.125407](https://doi.org/10.1103/PhysRevB.103.125407)**I. INTRODUCTION**

Quantum confinement endows two-dimensional (2D) layered materials with exceptional physics and novel properties compared to their bulk counterparts. Graphene is a well-known 2D material. Since it was first produced in 2004, more than 700 2D materials have been predicted to be stable [1,2]. Among them, only a few 2D materials possess the single-atom-thick monolayer, which is usually composed of the third to fifth group elements, such as graphene, silicene, borophene, and boron nitride [3–5]. Their typical structural pattern is the hexagonal honeycomb lattice and the  $sp^2$  orbital hybridization is the main force to stabilize the structure [6,7]. The electronic properties of the single-atom-thick 2D materials are dominated by the  $p$ -orbital electrons in the outmost shell of the third to fifth group elements. More importantly, their crystal field is a 2D crystal field with no atom lying above and below the monolayer and the electronic movement is confined in the 2D space. It is not only distinct to the crystal field in bulk compound, but also different from that in other slab 2D materials consisting of a few layers of atoms. Consequently, the uniqueness of the single-atom-thick geometry can bring about some exotic physical phenomena.

Transition-metal compounds usually have rich physical properties. One reason is that transition-metal elements have the  $d$  electronic shell with five partial  $d$  orbitals, which give rise to more orbital alignments and electron populations. On the other hand, spin is an important degree of freedom to determine the nature of transition-metal compounds, which interacts with lattice and charge degree to result in more complex physical phenomena such as magnetism and superconductivity [8,9].

The natural question is whether there exists a single-atom-thick 2D material containing transition-metal element, which

possesses the advantages of both single-atom-thick 2D compound and transition-metal compound. In a previous study, the 3d transition-metal monocarbides  $\text{TMC}$  ( $\text{TM} = \text{Co}, \text{Fe}, \text{Cu}, \text{etc.}$ ) and  $\text{CoB}_6$  with the planar monolayer structure were predicted by Larionov *et al.* [10,11] and Tang *et al.* [12]. Apart from this, the single-atom-thick 2D transition-metal compound has rarely been reported. The goal of our study is to design such a kind of material. The initial idea is that one can insert transition-metal atom into graphene directly, but the metal atom would rise from the graphene plane with a buckling height of about 0.5 Å [13]. Some experimental facts give us a lot of inspiration to solve the problem. First, nitrido-transition-metal complex is a class of coordination compounds that contain the nitrogen atom bound to transition metals, which demonstrates that N atom can play a role of bridge between transition metals and main group elements [14,15]. Second, the discovery of  $g\text{-C}_3\text{N}_4$  indicates that C and N atoms can be combined together to form a planar configuration [16]. Third, in the experiment of catalyst synthesis, more than 20 kinds of metal elements have been embedded in N-doped graphene to form  $\text{MN}_x$  graphene ( $M$  is metal) complexes [17,18], and a cascade anchoring strategy has been developed to synthesize the high-loading metal-nitrogen catalyst with a metal loading up to 12.1 wt% [19]. Moreover, the planar structure of  $\text{MN}_4$  moiety implanted in the graphene sheet has been definitely identified by the systematic x-ray absorption fine structure analyses and direct transmission electron microscopy imaging [20]. On the basis of these experiments and the above analysis, in this paper we design three kinds of 2D materials by assembling  $\text{CoN}_4$  moiety and several carbon atoms, which have a single-atom-thick plane and contain transition-metal element.

**II. COMPUTATIONAL DETAILS**

In our calculations, the plane wave pseudopotential method was used and implemented in Vienna *ab initio* simulation

\*yanxunwang@163.com

package (VASP) program [21,22]. The generalized gradient approximation (GGA) with Perdew-Burke-Ernzerhof (PBE) formula [23] as well as the projector augmented-wave method (PAW) [24] for ionic potential were employed. The plane wave basis cutoff was set to 600 eV and the convergence thresholds for the total energy and force were  $10^{-5}$  eV and  $0.001$  eV/Å. The Co-N-C monolayer lay in  $xy$  plane in the unit cell and the lattice parameter  $c$  was set to 16 Å to model the isolated monolayer. For the structural optimizations and self-consistent energy calculations, a mesh of  $16 \times 16 \times 1$   $k$  points were sampled for the Brillouin zone integration, which was less than  $2\pi \times 0.01/\text{Å}$  in reciprocal space for all the structures. We also take the electron correlation correction into account in the calculations and the GGA+U method is used with the Hubbard U values of 2, 4, and 6 eV. To inspect the kinetic stability of the Co-N-C monolayers, the phonon calculations were carried out with the supercell method in the PHONOPY program, and the real-space force constants of supercells were calculated using density-functional perturbation theory (DFPT) as implemented in VASP [25]. The strict force convergence criterion ( $10^{-6}$  eV/Å) was used in structural optimization of the primitive cell before building the supercell. The *ab initio* molecular dynamics (AIMD) simulations were performed to examine thermal stability. The  $3 \times 3 \times 1$  supercells were employed to minimize the constraint of periodic boundary conditions and the temperature was kept at 1000 K for 10 ps with a time step of 1 fs in the moles-volume-temperature (NVT) ensemble [26].

### III. RESULTS

#### A. Atomic structure

The  $\text{CoN}_4$  moiety is composed of one Co atom and four N atoms and the Co atom lies at the center of four N atoms. Since  $\text{CoN}_4$  unit has a planar configuration and the combination of N and C atoms in  $g\text{-C}_3\text{N}_4$  can keep in a plane, we can assemble the  $\text{CoN}_4$  unit and carbon atoms to constitute new 2D materials of cobalt carbonitride, in which N atoms play a bridge between Co and C atom. There are many arrangements of  $\text{CoN}_4$  units and carbon atoms, so various structural models are built. After a lot of trial and error, three representative structural models are found out, which are named  $\text{CoN}_4\text{C}_{10}$ ,  $\text{Co}_2\text{N}_8\text{C}_6$ , and  $\text{Co}_2\text{N}_6\text{C}_6$  in terms of their chemical formula. All three structures possess the rhombic lattice, and their plane symmetry group is  $C_{mm}$  with the plane group No. 4, affiliated to point group  $D_2$ . The detailed lattice parameters and atomic positions of three structures can be found in the *cif* files in the Supplemental Material [27].

Figures 1(a)–1(c) present the three structures with  $2 \times 1$  supercell, whose conventional crystal cell is marked by the solid line rectangle and the dashed line rhombus is the primitive cell. Each structural model is composed of two kinds of components, which are presented on the right side of the corresponding structure. The first model is  $\text{CoN}_4\text{C}_{10}$  shown in Fig. 1(a), which is made up of  $\text{CoN}_4$  unit and two-benzene-rings unit. In  $\text{CoN}_4\text{C}_{10}$ , the  $\text{CoN}_4$  units are separated by two-benzene-rings units and isolated from other  $\text{CoN}_4$  units. That is, at the edge of  $\text{CoN}_4$  unit, N atom is only connected

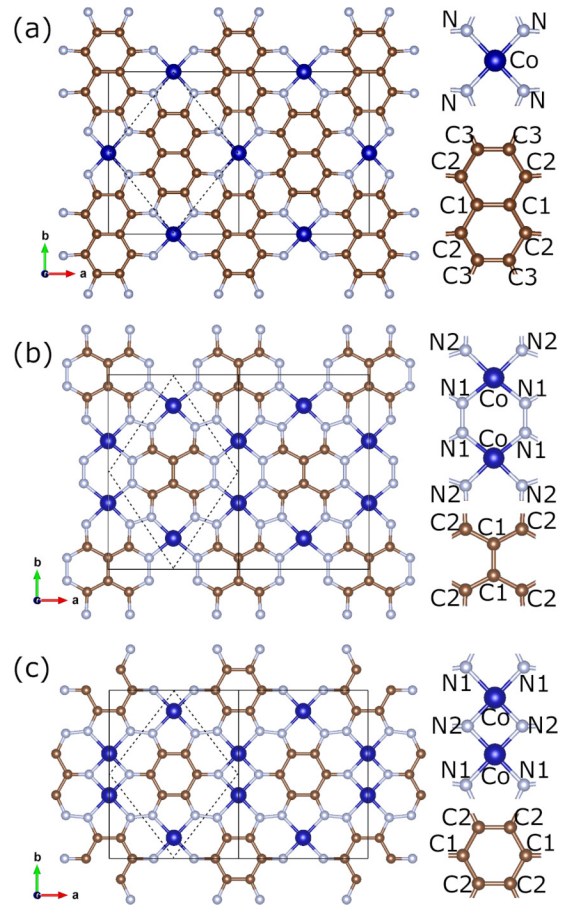


FIG. 1. Atomic structures of (a)  $\text{CoN}_4\text{C}_{10}$ , (b)  $\text{Co}_2\text{N}_8\text{C}_6$ , and (c)  $\text{Co}_2\text{N}_6\text{C}_6$  with the  $2 \times 1$  supercell. The conventional crystal cell is marked as a rectangle with the solid black line, and the dash line rhombus is the primitive cell. Each of the Co-N-C compounds is composed of two building blocks, which are shown in the right part of the panel. The nonequivalent N or C atom according to the group symmetry is named N1, N2, C1, C2, or C3.

to C atom. The second model  $\text{Co}_2\text{N}_8\text{C}_6$  is composed of the  $\text{CoN}_4$  unit and H-type unit of six carbon atoms, displayed in Fig. 1(b). Or more precisely, one component of  $\text{Co}_2\text{N}_8\text{C}_6$  is the block of two  $\text{CoN}_4$  units with the side-by-side alignment and the other is the H-type unit of six carbon atoms. In  $\text{Co}_2\text{N}_8\text{C}_6$ , N atom is connected to one C atom and one N atom at the edge of  $\text{CoN}_4$  unit. In the third model  $\text{Co}_2\text{N}_6\text{C}_6$  in Fig. 1(c), two  $\text{CoN}_4$  units are fused together to form a block of  $\text{Co}_2\text{N}_6$  by two shared N atoms, and the whole sheet contains the  $\text{Co}_2\text{N}_6$  block and the benzene-ring unit. In  $\text{Co}_2\text{N}_6\text{C}_6$ , some of N atoms are bonded to two Co atoms. In addition, the two-benzene-rings unit, H-type unit, and benzene-ring unit can be considered as the different graphene fragments, thus the structures of  $\text{CoN}_4\text{C}_{10}$ ,  $\text{Co}_2\text{N}_8\text{C}_6$ , and  $\text{Co}_2\text{N}_6\text{C}_6$  are made up of the  $\text{CoN}_4$  unit and the graphene fragment. For the convenience to describe the charge distribution and transfer in the following section, the nonequivalent N or C atoms in the structural unit are labeled as N1, N2, C1, C2, or C3, see the right panels of Figs. 1(a)–1(c).

## B. Structural stability

To ascertain the structural stability of the three structural models, we perform the calculations of cohesive energy, formation energy, phonon spectra, and molecular dynamics, and then the stabilization mechanism of  $\text{CoN}_4\text{C}_{10}$ ,  $\text{Co}_2\text{N}_8\text{C}_6$ , and  $\text{Co}_2\text{N}_6\text{C}_6$  is discussed.

### 1. Cohesive energy and formation energy

The average cohesive energy  $\bar{E}_{\text{coh}}$  is defined as

$$\bar{E}_{\text{coh}} = \frac{1}{n} * \left( E_{\text{tot}} - \sum_i E_{\text{atom}(i)} * n_i \right), \quad (1)$$

in which  $E_{\text{tot}}$  is the total energy;  $E_{\text{atom}(i)}$  is the single atom energy for Co, N, or C element;  $n$  is the total atomic number and  $n_i$  is the atomic number for a specific element. The average cohesive energies for  $\text{CoN}_4\text{C}_{10}$ ,  $\text{Co}_2\text{N}_8\text{C}_6$ , and  $\text{Co}_2\text{N}_6\text{C}_6$  are  $-7.00$  eV/atom,  $-6.07$  eV/atom, and  $-6.20$  eV/atom, respectively. For comparison, the cohesive energies of graphene, silicene and  $\text{MoS}_2$  monolayer are also calculated, and the values are  $-7.96$  eV/atom,  $-3.96$  eV/atom, and  $-5.14$  eV/atom, which are consistent with the ones in previous studies [28,29]. The lower the cohesive energy value, the more stable the material. So, from the view of cohesive energy,  $\text{CoN}_4\text{C}_{10}$ ,  $\text{Co}_2\text{N}_8\text{C}_6$ , and  $\text{Co}_2\text{N}_6\text{C}_6$  are more stable than silicene and  $\text{MoS}_2$  monolayer.

Next, we compute their formation energies of  $\text{CoN}_4\text{C}_{10}$ ,  $\text{Co}_2\text{N}_8\text{C}_6$ , and  $\text{Co}_2\text{N}_6\text{C}_6$ . We take graphene, metal cobalt, and  $g\text{-C}_3\text{N}_4$  as the reference materials [16], which are already existing or have been synthesized in experiments. The formation energy is defined below,

$$\begin{aligned} E_{\text{form}}(\text{CoN}_4\text{C}_{10}) &= E_{\text{tot}} - E_{\text{Co}} - E_{\text{C}_3\text{N}_4} - 7E_{\text{C}} \\ &= -0.86 \text{ eV}, \\ E_{\text{form}}(\text{Co}_2\text{N}_8\text{C}_6) &= E_{\text{tot}} - 2E_{\text{Co}} - 2E_{\text{C}_3\text{N}_4} \\ &= -1.73 \text{ eV}, \\ E_{\text{form}}(\text{Co}_2\text{N}_6\text{C}_6) &= E_{\text{tot}} - 2E_{\text{Co}} - 1.5E_{\text{C}_3\text{N}_4} - 1.5E_{\text{C}} \\ &= -2.04 \text{ eV}. \end{aligned} \quad (2)$$

$E_{\text{form}}$ ,  $E_{\text{Co}}$ ,  $E_{\text{C}_3\text{N}_4}$ , and  $E_{\text{C}}$  are the formation energy, the metal energy per Co atom, the  $g\text{-C}_3\text{N}_4$  energy per formula cell, and the graphene energy per carbon atom, respectively. For the three 2D monolayers, the negative value indicates an energy decrease in the formation of them using these reference materials as reactants. Namely, it is energetically favorable to synthesize them. To compare the stability of the three predicted structures and  $g\text{-C}_3\text{N}_4$ , we also compute their average formation energies per atom starting from cobalt metal, graphene, and  $\text{N}_2$  molecule. The average formation energies are  $0.047$  eV/atom,  $0.176$  eV/atom, and  $0.199$  eV/atom for  $\text{CoN}_4\text{C}_{10}$ ,  $\text{Co}_2\text{N}_8\text{C}_6$ , and  $\text{Co}_2\text{N}_6\text{C}_6$ , while the energy is  $0.346$  eV/atom for  $g\text{-C}_3\text{N}_4$ . From the viewpoint of formation energy, the stability of the three predicted structures is at least comparable to the stability of  $g\text{-C}_3\text{N}_4$ .

### 2. Phonon spectra and molecular dynamic simulation

Phonon spectrum is an important means to judge the structural stability of solid materials. Based on the DFPT method

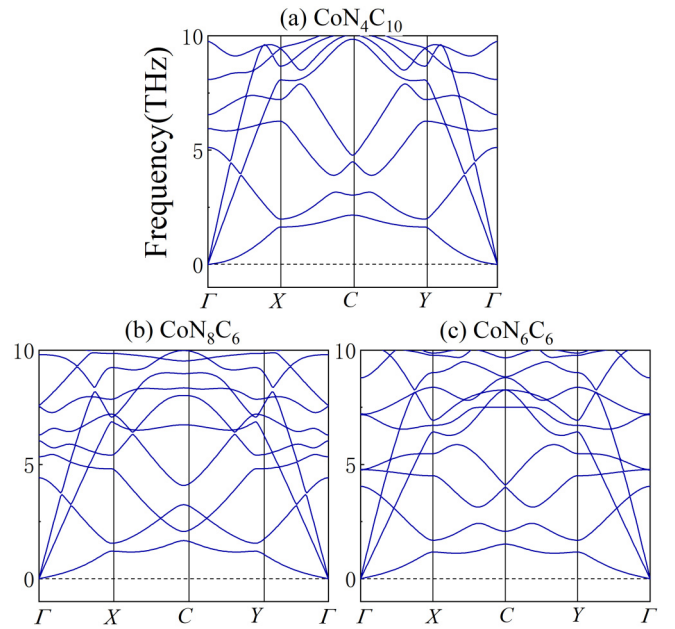


FIG. 2. Phonon spectra of (a)  $\text{CoN}_4\text{C}_{10}$ , (b)  $\text{Co}_2\text{N}_8\text{C}_6$ , and (c)  $\text{Co}_2\text{N}_6\text{C}_6$  in ferromagnetic ordering phase. The  $k$  path along high symmetry axes in reciprocal space is same to that in energy band calculations, see the following Fig. 5.

in VASP code, we have investigated the phonon spectra of  $\text{CoN}_4\text{C}_{10}$ ,  $\text{Co}_2\text{N}_8\text{C}_6$ , and  $\text{Co}_2\text{N}_6\text{C}_6$  along the high-symmetry  $k$  path in Brillouin zone. The phonon spectra are shown in Fig. 2, in which the special  $k$  points are the same as in Fig. 5. If there exists an unstable phonon mode, it is presented as an imaginary frequency. No imaginary frequency appears in Fig. 2, which confirms the kinetic stability of three Co-N-C structures. Then, we perform the first-principles molecular dynamic simulations to examine their thermal stability. The simulations are carried out at the temperature of  $1000$  K and with the time of  $10$  ps. The results show that  $\text{CoN}_4\text{C}_{10}$ ,  $\text{Co}_2\text{N}_8\text{C}_6$ , and  $\text{Co}_2\text{N}_6\text{C}_6$  can maintain their framework and no breaking of the bonds is found, which demonstrates that all of three monolayer structures have good thermal stability.

### 3. Stabilization mechanism

For the stability mechanism, the first thing we notice is the arrangement of C and N atoms, which is similar to the honeycomb structure of graphene or  $g\text{-C}_3\text{N}_4$ . In these Co-N-C monolayers, all C and N atoms are tricoordinated and linked to the neighboring C, N, or Co atoms, making up of the basic framework of the planar structure. Carbon atom has four valence electrons and three of them occupy three  $sp^2$  hybrid orbitals, which are combined with the  $sp^2$  orbitals of the neighboring C and N atoms to form three  $\sigma$  bonds. Nitrogen atoms also have three  $sp^2$  orbitals, but one is connected to  $d$  orbital of cobalt atom to form the ionic bond and other two are linked to  $sp^2$  orbitals from C or N atom to form the covalence bond. As for the  $p_z$  orbitals of C and N atoms, they are oriented perpendicularly to the plane and hybridize together to form the  $\pi$  bond, which extends over the whole monolayer and further stabilizes the planar geometry. Co atom is situated

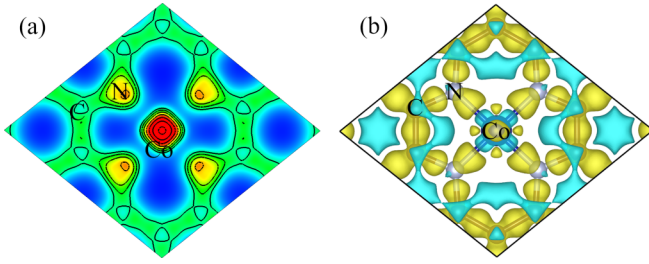


FIG. 3. (a) 2D charge density in atomic plane of  $\text{CoN}_4\text{C}_{10}$ . (b) charge density difference of  $\text{CoN}_4\text{C}_{10}$  relative to the superposition of atomic charge density. In the left panel, charge density increases with color varying from blue to red. In the right panel, yellow and blue surfaces show charge accumulation and depletion, respectively.

at the center of four N atoms and is confined in the plane by the four ionic Co-N bonds. We take  $\text{CoN}_4\text{C}_{10}$  as an example to analyze the charge distribution and difference charge density. Figure 3(a) exhibits the 2D charge density in the monolayer plane where the charge density increases from blue to red and the black lines are the isocontours. There is less charge in the middle of Co and N atoms, while the side of N atom has the denser contour lines, indicating higher charge density at the side of N atom. There is a fairly uniform distribution of charge between C-C atoms and C-N atoms, corresponding to the covalent C-C and C-N bonds. Figure 3(b) displays the charge density difference relative to the superposition of atomic charge density. Yellow and blue surfaces show positive and negative values, respectively. The yellow surface at the side of N atom shows the charge transfer from Co to N atoms along Co-N line, forming the Co-N ionic bond. The charge is accumulated obviously between C-C atoms and C-N atoms, resulting in the C-N and C-C covalent bonds.

### C. Electronic structure

#### 1. Charge transfer

By the Bader charge method [30], we quantitatively compute the charge transfer among Co, N, and C atoms in these Co-N-C monolayers and list them in Table I. The positive and negative values mean the charge gain or loss, respectively. The charge loss of Co atoms is  $0.85 \sim 0.90$  electron in three Co-N-C compounds, and the charge gain of N atoms is from  $0.28 \sim 0.64$  electron. With different positions and coordination environments, the charge of C atoms has a significant difference. The lost charges of  $\text{C}_2$  atoms in  $\text{CoN}_4\text{C}_{10}$  and  $\text{Co}_2\text{N}_6\text{C}_6$

TABLE I. The charge accumulation and depletion of Co, N, and C atom in  $\text{CoN}_4\text{C}_{10}$ ,  $\text{Co}_2\text{N}_8\text{C}_6$ , and  $\text{Co}_2\text{N}_6\text{C}_6$  relative to the charge of single isolated atom. The atom labels are marked as  $\text{C}_1$ ,  $\text{C}_2$ ,  $\text{C}_3$ ,  $\text{N}_1$ , and  $\text{N}_2$  according to the space group symmetry, displayed in the right panel of Fig. 1. Short dashed line means no existence of such atoms.

phases	Co	$\text{N}_1$	$\text{N}_2$	$\text{C}_1$	$\text{C}_2$	$\text{C}_3$
$\text{CoN}_4\text{C}_{10}$	-0.85	+0.39	-	+0.01	-0.11	-0.07
$\text{Co}_2\text{N}_8\text{C}_6$	-0.86	+0.54	+0.51	+0.14	-0.69	-
$\text{Co}_2\text{N}_6\text{C}_6$	-0.90	+0.28	+0.64	-0.17	-0.07	-

are 0.07 and 0.11 electron, while the value of  $\text{C}_2$  atom in  $\text{Co}_2\text{N}_8\text{C}_6$  reaches up to 0.69 electron due to link to two N atoms. And for the  $\text{C}_1$  atoms in  $\text{CoN}_4\text{C}_{10}$  and  $\text{Co}_2\text{N}_8\text{C}_6$ , the charge gains are 0.01 and 0.14 electron, respectively. In general, the charge is transferred from Co atom and C atom to N atom for all the Co-N and C-N bonds in these Co-N-C compounds due to the strong electronegativity of N element.

#### 2. Density of states

The spin polarization calculations show the moments of Co atoms in  $\text{CoN}_4\text{C}_{10}$ ,  $\text{Co}_2\text{N}_8\text{C}_6$ , and  $\text{Co}_2\text{N}_6\text{C}_6$  are 0.93, 0.25, and  $0.88 \mu_B$ , respectively. Even though there is the same tetra-coordinate Co atom with four N atoms, the difference of the Co moments in three 2D compounds is obvious, which indicates that besides the ligand field formed by the neighbored N atoms, the chemical stoichiometric ratio of Co, N, and C element and the next neighbored atoms have a great influence on the spin polarization of Co 3d electrons. The difference of magnetic moments around Co atoms is explained by their spin-polarized density of states (DOS) shown in top panels of Figs. 4(a)–4(c). Comparing the DOS of  $\text{Co}_2\text{N}_8\text{C}_6$  with the DOS spectra of other two systems, we find that the charge of  $\text{Co}_2\text{N}_8\text{C}_6$  has the least spin polarization, resulting in the small magnetic moment.

Next, we examine the effect of parallel and antiparallel alignment of magnetic moments on the energy of the system. The primitive cells of  $\text{Co}_2\text{N}_8\text{C}_6$  and  $\text{Co}_2\text{N}_6\text{C}_6$  contain two Co atoms. When the two Co moments of  $\text{Co}_2\text{N}_8\text{C}_6$  and  $\text{Co}_2\text{N}_6\text{C}_6$  are aligned in the parallel pattern, their energies is 4 meV and 130 meV lower than the energies in the case of antiparallel pattern, respectively. Due to only one Co atom in the primitive cell of  $\text{CoN}_4\text{C}_{10}$ , the conventional cell shown in Fig. 1(a) is used to inspect the energy difference of parallel and antiparallel alignment of two Co moments. The energy of antiparallel alignment is 2.8 meV per formula cell lower than the energy of parallel alignment. For the sake of comparison of electronic properties, we adopt the primitive cell with ferromagnetic ordering to calculate the electronic structures of  $\text{CoN}_4\text{C}_{10}$ ,  $\text{Co}_2\text{N}_8\text{C}_6$ , and  $\text{Co}_2\text{N}_6\text{C}_6$ .

In Fig. 4, the projected DOS spectra of Co 3d, N 2p, and C 2p of the three Co-N-C monolayers are plotted. The electronic states of N 2p and C 2p orbitals mainly distribute the same energy range of  $-10 \text{ eV} \sim -4 \text{ eV}$ , and the strong hybridization of N 2p and C 2p orbitals leads to the strong C-N bonds to stabilize the framework of these Co-N-C monolayers. In the vicinity of Fermi energy (from  $-2 \text{ eV}$  to  $2 \text{ eV}$ ), the DOS peaks of Co 3d orbitals coincide with the peaks of N 2p orbital, which, combined with the fact that 0.85, 0.90 electron of Co atom is transferred to N atoms, indicates that there is a strong bond between N and Co atoms. We remind that the vertical axes of the top figures have a much larger range than the ones in two panels below. For three Co-N-C two-dimensional materials, there are two features of electronic structure that deserve special attention. First, their electronic states near the Fermi level are dominated by the electrons of Co 3d orbitals, which denotes that  $\text{CoN}_4\text{C}_{10}$ ,  $\text{Co}_2\text{N}_8\text{C}_6$ , and  $\text{Co}_2\text{N}_6\text{C}_6$  monolayers have the typical electronic character of 3d transition-metal compounds. The material with both the single-atom-thickness and the 3d electronic character is rare in 2D materials. Second,

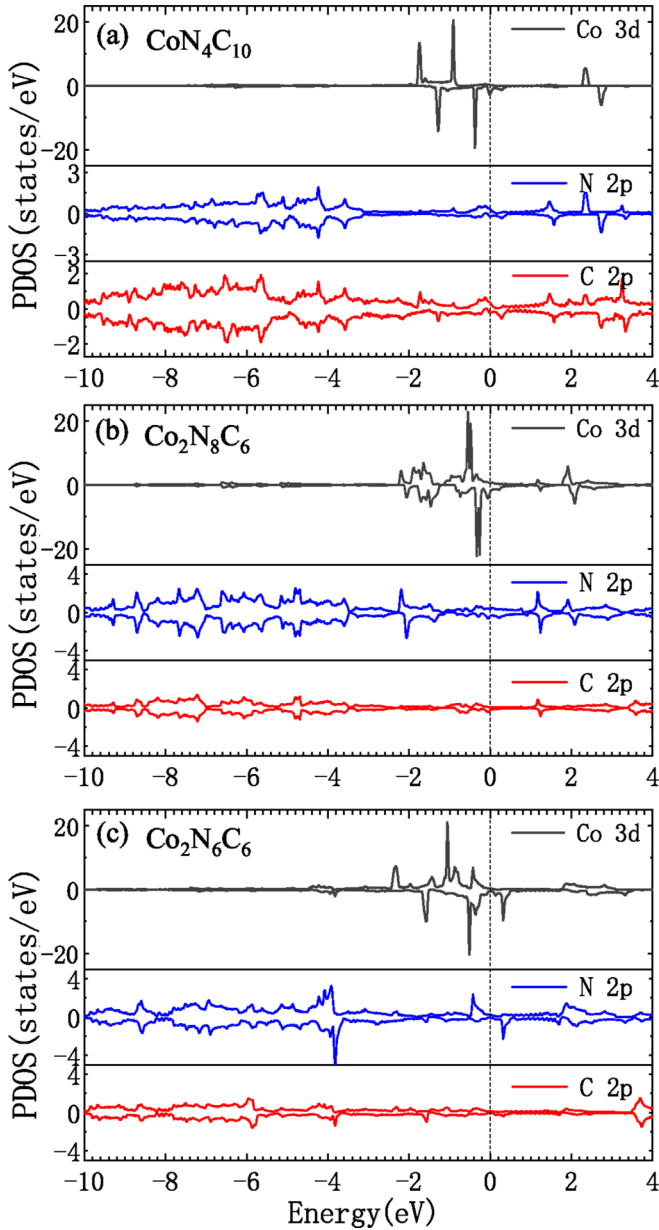


FIG. 4. The projected DOS on the atomic orbitals of (a)  $\text{CoN}_4\text{C}_{10}$ , (b)  $\text{Co}_2\text{N}_8\text{C}_6$ , and (c)  $\text{Co}_2\text{N}_6\text{C}_6$ . The vertical axis of top panel in (a), (b), or (c) has a much larger range of density of states than two panels below. It is noted that the sharp DOS peaks of Co 3d states are much higher than the ones of N and C 2p states in the three kinds of cobalt carbonitrides. The Fermi energy is set to zero.

for each of three Co-N-C 2D compounds, their DOS curves have two sharp DOS peaks more than 20 states/eV, which are located at  $-0.8$  eV and  $-0.4$  eV,  $-0.4$  eV and  $-0.2$  eV, and  $-1.0$  eV and  $-0.5$  eV in Figs. 4(a), 4(b), and 4(c), respectively. These sharp DOS peaks are found to originate from the  $d_{z^2}$  partial orbitals when Co 3d states are divided into five partial  $d$  orbitals. The reason is that Co  $d_{z^2}$  orbital is vertical to the 2D monolayer and does not hybridize with other atomic orbitals along  $z$  direction. Because the appearance of the sharp DOS peaks is tightly related to the reduced dimension of

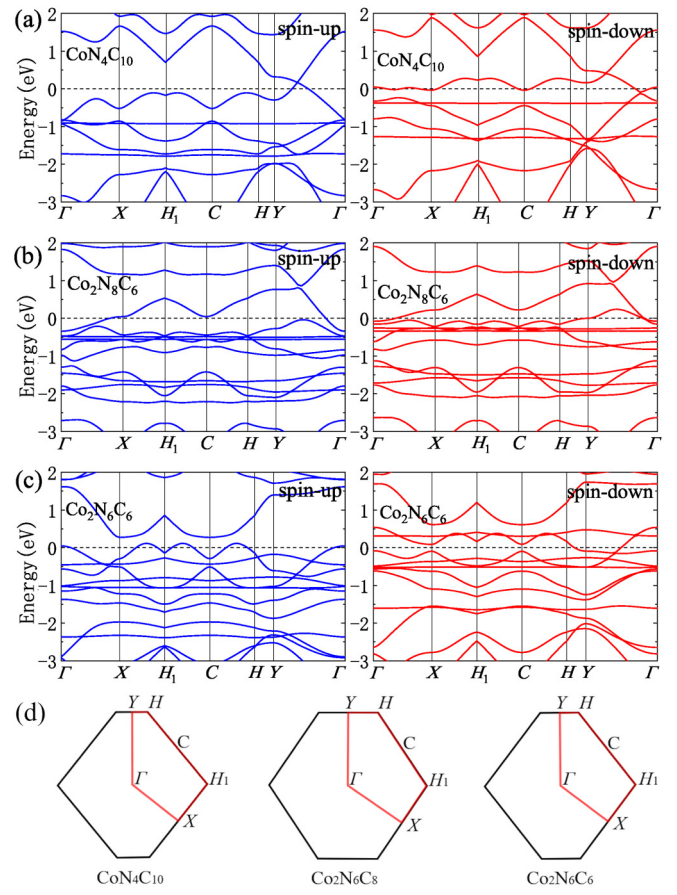


FIG. 5. Band structures of (a)  $\text{CoN}_4\text{C}_{10}$ , (b)  $\text{Co}_2\text{N}_8\text{C}_6$ , and (c)  $\text{Co}_2\text{N}_6\text{C}_6$  in ferromagnetic phase. The blue lines are spin-up electronic bands and the red lines correspond to spin-down electronic bands. (d) the Brillouin zones and high-symmetric  $k$  points.

these Co-N-C monolayers, such sharp peaks can hardly be found in bulk materials. Consequently, the two features of electronic structure mentioned above make the three Co-N-C 2D materials distinct from other materials.

### 3. Band structure

The band structures of  $\text{CoN}_4\text{C}_{10}$ ,  $\text{Co}_2\text{N}_8\text{C}_6$ , and  $\text{Co}_2\text{N}_6\text{C}_6$  and the corresponding Brillouin zone are displayed in Figs. 5(a), 5(b), 5(c), and 5(d), where two or three bands cross their Fermi levels, revealing that all three 2D monolayers are metallic. The red lines are related to spin-up bands and the blue lines are spin-down bands. In the band structures of  $\text{CoN}_4\text{C}_{10}$ ,  $\text{Co}_2\text{N}_8\text{C}_6$ , and  $\text{Co}_2\text{N}_6\text{C}_6$ , the most striking feature is the appearance of the flat energy bands, which are related to the sharp peaks in DOS spectra. The sharp DOS peaks and the flat bands are from the Co 3d electrons. Twisted bilayer graphene with a magic angle  $\sim 1.08^\circ$  shows flat bands at Fermi energy and has recently attracted great attention from researchers, in which the superconductivity can be achieved by the gate voltage tunability [31,32]. However, the complex experimental techniques are required to control the twist angle  $\sim 1.08^\circ$ . By contrast, the flat bands in  $\text{CoN}_4\text{C}_{10}$ ,  $\text{Co}_2\text{N}_8\text{C}_6$ , and  $\text{Co}_2\text{N}_6\text{C}_6$  can be easily obtained and they are very close to Fermi energy, especially only 0.26 eV for  $\text{Co}_2\text{N}_8\text{C}_6$ . So these

TABLE II. The lattice parameters, the magnetic moment around Co atoms, and the charge loss of Co atoms for  $\text{CoN}_4\text{C}_{10}$ ,  $\text{Co}_2\text{N}_8\text{C}_6$ , and  $\text{Co}_2\text{N}_6\text{C}_6$  without and with Hubbard  $U$ .

$\text{CoN}_4\text{C}_{10}$	$a$	$\theta$	Co moment	Co charge
$U = 0$	6.480 Å	102.417°	0.93 $\mu_B$	-0.85 e
$U = 2$	6.501 Å	102.436°	1.01 $\mu_B$	-0.93 e
$U = 4$	6.505 Å	102.421°	1.01 $\mu_B$	-0.98 e
$U = 6$	6.511 Å	102.404°	1.02 $\mu_B$	-0.96 e
$\text{Co}_2\text{N}_8\text{C}_6$	$a$	$\theta$	Co moment	Co charge
$U = 0$	7.016 Å	112.254°	0.25 $\mu_B$	-0.86 e
$U = 2$	7.049 Å	112.125°	0.75 $\mu_B$	-0.80 e
$U = 4$	7.081 Å	112.098°	1.00 $\mu_B$	-0.92 e
$U = 6$	7.096 Å	112.007°	1.00 $\mu_B$	-0.92 e
$\text{Co}_2\text{N}_6\text{C}_6$	$a$	$\theta$	Co moment	Co charge
$U = 0$	6.476 Å	104.877°	0.88 $\mu_B$	-0.90 e
$U = 2$	6.545 Å	106.286°	1.02 $\mu_B$	-0.98 e
$U = 4$	6.554 Å	106.339°	1.01 $\mu_B$	-0.98 e
$U = 6$	6.562 Å	106.299°	1.01 $\mu_B$	-0.94 e

Co-N-C 2D compounds are the new and more convenient platforms to study the physics related to the flat band.

#### 4. Electron correlation

To inspect the electron correlation effect on the electronic properties of  $\text{CoN}_4\text{C}_{10}$ ,  $\text{Co}_2\text{N}_8\text{C}_6$ , and  $\text{Co}_2\text{N}_6\text{C}_6$  compounds, we use the GGA +  $U$  method to recalculate their electronic structures. The Hubbard  $U$  is set to 2, 4, and 6 eV to estimate the correlation strength, and the optimized lattice parameters, magnetic moment around Co atom, and the charge loss of Co atom are listed in Table II. With Hubbard  $U$  varying from 0–6 eV, the maximum changes of lattice parameter  $a$  of  $\text{CoN}_4\text{C}_{10}$ ,  $\text{Co}_2\text{N}_8\text{C}_6$ , and  $\text{Co}_2\text{N}_6\text{C}_6$  are 0.031 Å, 0.080 Å, and 0.086 Å, respectively, and the maximum changes of angle  $\theta$  between two lattice vectors of the rectangle cell are 0.032°, 0.247°, and 1.462°. The results indicate that the  $U$  values have little effect on the optimized lattice parameters. As for the charge loss and magnetic moment of Co atom, they show an increasing trend with the variation of  $U$  values from 0–6 eV. When  $U$  value is larger than 2 eV for  $\text{CoN}_4\text{C}_{10}$  and  $\text{Co}_2\text{N}_6\text{C}_6$  and 4 eV for  $\text{Co}_2\text{N}_8\text{C}_6$ , the lost charge of Co atom is close to one electron and the magnetic moment is close to 1  $\mu_B$ .

With the Hubbard  $U$  of 2, 4, and 6 eV, the projected DOS on Co  $d$  orbitals are calculated for  $\text{CoN}_4\text{C}_{10}$ ,  $\text{Co}_2\text{N}_8\text{C}_6$ , and  $\text{Co}_2\text{N}_6\text{C}_6$  and shown in Fig. 6. Without Hubbard  $U$ , the Co  $d$  orbitals are distributed in the range of  $-2.0 \sim 0$  eV for  $\text{CoN}_4\text{C}_{10}$ . With the Hubbard  $U$  increasing from 2, 4, to 6 eV, the energy ranges are  $-3.0 \sim 0$  eV,  $-3.5 \sim 0$  eV, and  $-4.0 \sim 0$  eV. Namely the energy range of  $d$  orbitals become more and more wide with Hubbard  $U$  increasing. The sharp DOS peak at  $-0.4$  eV in Fig. 4(a) are gradually shifted to  $-0.3$ , 0, and 0.1 eV in Fig. 6(a) with  $U = 2, 4$ , and 6 eV. After the electron correlation effect is included in the calculations, the sharp DOS peaks are still located in the vicinity of Fermi energy. Similarly, there are flat bands near the Fermi energy in the band structure of  $\text{CoN}_4\text{C}_{10}$ , which is related to the sharp

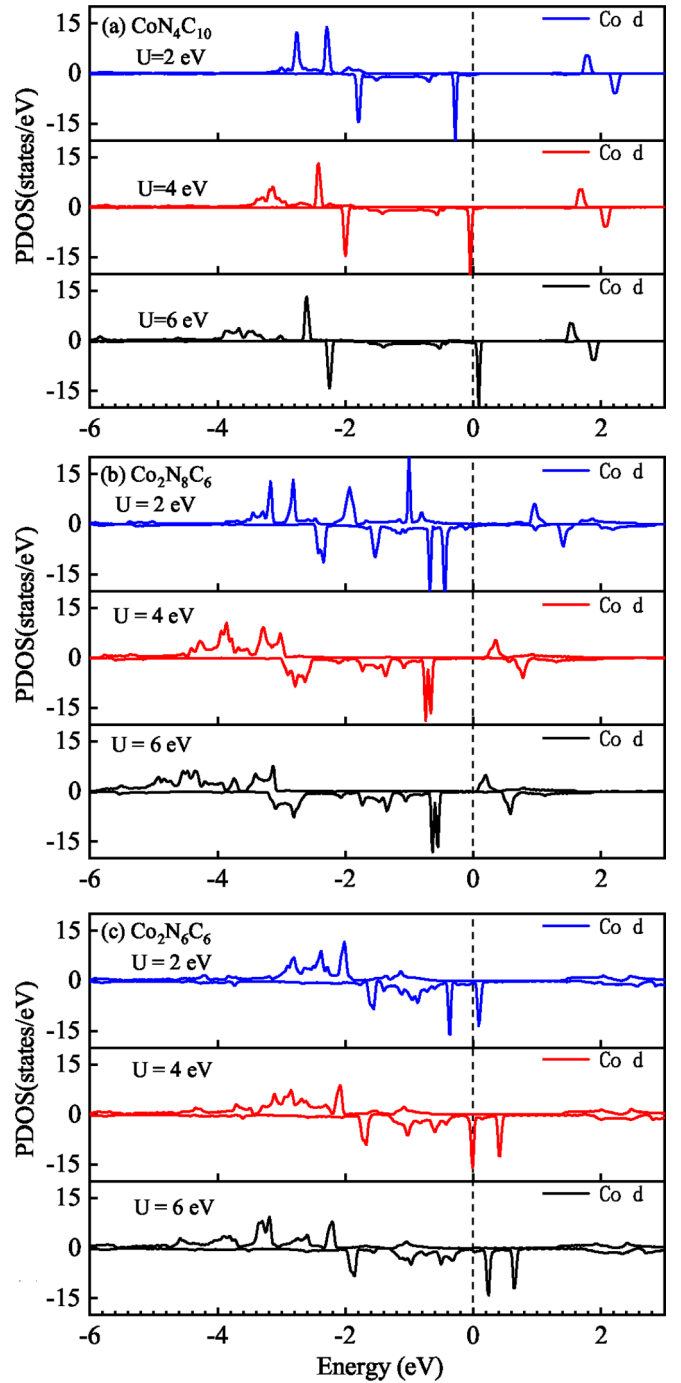


FIG. 6. The projected DOS on  $d$  orbitals of Co atom are shown for (a)  $\text{CoN}_4\text{C}_{10}$ , (b)  $\text{Co}_2\text{N}_8\text{C}_6$ , and (c)  $\text{Co}_2\text{N}_6\text{C}_6$  in the ferromagnetic phase. The Hubbard  $U$  values of 2, 4, and 6 eV are used in the GGA+ $U$  calculations, and the corresponding projected DOS of Co  $d$  orbitals are displayed with the blue, red, and black lines in the top, middle, and bottom panels for each of the three cobalt carbonitride compounds. The Fermi energy is set to zero and is marked as a vertical dashed line.

DOS peaks. For  $\text{Co}_2\text{N}_8\text{C}_6$  monolayer, the distribution range of  $d$  orbitals has been obviously extended after the Hubbard  $U$  is considered, which varies from  $-2.0 \sim 0$  eV without Hubbard  $U$ , to  $-3.6 \sim -0.4$  eV with  $U = 2$  eV,  $-4.4 \sim -0.6$  eV

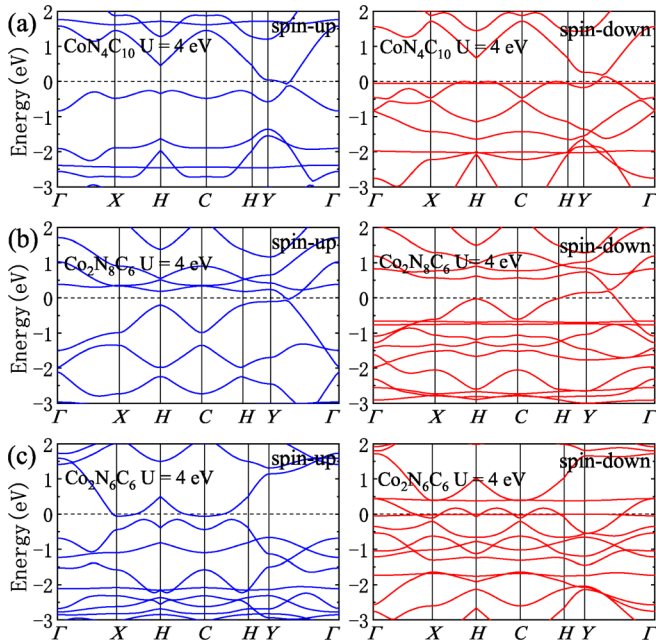


FIG. 7. Band structures of (a)  $\text{CoN}_4\text{C}_{10}$ , (b)  $\text{Co}_2\text{N}_8\text{C}_6$ , and (c)  $\text{Co}_2\text{N}_6\text{C}_6$  are from the GGA+U calculation with  $U = 4$  eV. The blue lines are spin-up electronic bands and the red lines correspond to spin-down electronic bands. The Brillouin zones and high symmetric  $k$  points are shown in Fig. 5.

with  $U = 4$  eV, and  $-5.5 \sim -0.5$  eV. In the spin-down DOS curves for  $U = 2, 4$ , and  $6$  eV, the sharp peaks lie in the region of  $-0.8 \sim -0.4$  eV and their positions have not changed much. For the  $d$ -orbital DOS of  $\text{Co}_2\text{N}_6\text{C}_6$  with Hubbard  $U$ , the variation of the energy range is similar to the ones of  $\text{CoN}_4\text{C}_{10}$  and  $\text{Co}_2\text{N}_8\text{C}_6$ . But the peaks of spin-down DOS move more to the right compared to the situation of  $\text{CoN}_4\text{C}_{10}$ , reaching to  $0.7$  eV above the Fermi energy. Figure 7 exhibits the band structures of  $\text{CoN}_4\text{C}_{10}$ ,  $\text{Co}_2\text{N}_8\text{C}_6$ , and  $\text{Co}_2\text{N}_6\text{C}_6$ , which come from the GGA+U calculation with  $U = 4$  eV. We take the situation of  $U = 4$  eV as an example to show the band structures with the electron correlation effect. For  $\text{CoN}_4\text{C}_{10}$  and  $\text{Co}_2\text{N}_6\text{C}_6$ , the flat bands are very close to Fermi energy or located at Fermi energy, while the flat band appear at about  $-0.7$  eV for  $\text{Co}_2\text{N}_8\text{C}_6$ . These flat bands correspond to the sharp DOS peaks in Fig. 6 and stem from the Co  $d_{z^2}$  electronic states. Apart from the flat bands, there are some crossing points very close to the Fermi level in spin-up and

spin-down bands of  $\text{CoN}_4\text{C}_{10}$ ,  $\text{Co}_2\text{N}_8\text{C}_6$  in Figs. 7(a) and 7(b). These crossing points also exist in the band structures of  $\text{CoN}_4\text{C}_{10}$ ,  $\text{Co}_2\text{N}_8\text{C}_6$  without Hubbard  $U$  in Figs. 5(a) and 5(b), which indicate that to some extent  $\text{CoN}_4\text{C}_{10}$  and  $\text{Co}_2\text{N}_8\text{C}_6$  have similar electronic features to graphene due to the partial similarity of their structures.

#### IV. CONCLUSIONS AND DISCUSSION

Based on the first-principles calculations, we predict three kinds of graphenelike Co-N-C 2D materials containing transition-metal cobalt. By calculating the cohesive energy, formation energy, phonon spectra, and molecular dynamics of  $\text{CoN}_4\text{C}_{10}$ ,  $\text{Co}_2\text{N}_8\text{C}_6$ , and  $\text{Co}_2\text{N}_6\text{C}_6$ , their structural stability has been determined. The cobalt content of the materials results in their rich electrical properties. The DOS near Fermi energy is dominated by Co  $3d$  electronic states and there exist sharp DOS peaks and flat bands in the vicinity of Fermi energy. After Hubbard  $U$  up to  $6$  eV being considered, the sharp DOS peaks and flat bands still exist around Fermi energy. The features make the single-atom-thick Co-N-C compounds distinct from other 2D materials and bulk compounds. Consequently, the predicted Co-N-C compounds are not only a new class of 2D materials but also an ideal platform to study the interaction among charge, spin, and lattice degrees in 2D compounds.

Moreover, three questions are worth considering. Apart from  $\text{CoN}_4\text{C}_{10}$ ,  $\text{Co}_2\text{N}_8\text{C}_6$ , and  $\text{Co}_2\text{N}_6\text{C}_6$ , there must exist many other arrangements of  $\text{CoN}_4$  units and carbon atoms to form the single-atom-thick 2D structure. Apart from  $\text{CoN}_4$  unit, other  $M\text{N}_4$  moieties such as  $\text{FeN}_4$ ,  $\text{NiN}_4$ ,  $\text{CuN}_4$ , etc. can also be combined with various fragments of graphene to form the single-atom-thick 2D structure. Third, the  $M$ -N-C ( $M = \text{Co}, \text{Fe}, \text{Cu}$ , etc.) 2D compounds are highly probable to be achieved or even have been achieved in experiments, because most transition metals have already been used to fabricate the  $M\text{N}_4$ -graphene complexes in the synthesis of single-atom catalysts [17,19]. From this viewpoint, our findings open a small window on a new large class of 2D materials.

#### ACKNOWLEDGMENT

This work was supported by the National Natural Science Foundation of China under Grants No. 11974207, No. 11974194, and No. 11474004.

- [1] K. S. Novoselov, *Science* **306**, 666 (2004).
- [2] M. Ashton, J. Paul, S. B. Sinnott, and R. G. Hennig, *Phys. Rev. Lett.* **118**, 106101 (2017).
- [3] B. Lalmi, H. Oughaddou, H. Enriquez, A. Kara, S. Vizzini, B. Ealet, and B. Aufray, *Appl. Phys. Lett.* **97**, 223109 (2010).
- [4] A. J. Mannix, X.-F. Zhou, B. Kiraly, J. D. Wood, D. Alducin, B. D. Myers, X. Liu, B. L. Fisher, U. Santiago, J. R. Guest, M. J. Yacaman, A. Ponce, A. R. Oganov, M. C. Hersam, and N. P. Guisinger, *Science* **350**, 1513 (2015).
- [5] L. Song, L. Ci, H. Lu, P. B. Sorokin, C. Jin, J. Ni, A. G. Kvashnin, D. G. Kvashnin, J. Lou, B. I. Yakobson, and P. M. Ajayan, *Nano Lett.* **10**, 3209 (2010).
- [6] H. Şahin, S. Cahangirov, M. Topsakal, E. Bekaroglu, E. Akturk, R. T. Senger, and S. Ciraci, *Phys. Rev. B* **80**, 155453 (2009).
- [7] C. Kamal and M. Ezawa, *Phys. Rev. B* **91**, 085423 (2015).
- [8] J. G. Bednorz and K. A. Müller, *Z. Phys. B: Condens. Matter* **64**, 189 (1986).
- [9] Y. Kamihara, T. Watanabe, M. Hirano, and H. Hosono, *J. Am. Chem. Soc.* **130**, 3296 (2008).

- [10] K. V. Larionov, Z. I. Popov, M. A. Vysotin, D. G. Kvashnin, and P. B. Sorokin, *JETP Lett.* **108**, 13 (2018).
- [11] K. V. Larionov, G. Seifert, and P. B. Sorokin, *Nanoscale* **12**, 13407 (2020).
- [12] X. Tang, W. Sun, Y. Gu, C. Lu, L. Kou, and C. Chen, *Phys. Rev. B* **99**, 045445 (2019).
- [13] A. V. Krasheninnikov, P. O. Lehtinen, A. S. Foster, P. Pyykkö, and R. M. Nieminen, *Phys. Rev. Lett.* **102**, 126807 (2009).
- [14] K. Dehnicke and J. Strähle, *Angew. Chem., Int. Ed. Engl.* **31**, 955 (1992).
- [15] K. Dehnicke, F. Weller, and J. Strähle, *Chem. Soc. Rev.* **30**, 125 (2001).
- [16] M. Groenewolt and M. Antonietti, *Adv. Mater.* **17**, 1789 (2005).
- [17] X. He, Q. He, Y. Deng, M. Peng, H. Chen, Y. Zhang, S. Yao, M. Zhang, D. Xiao, D. Ma, B. Ge, and H. Ji, *Nat. Commun.* **10**, 3663 (2019).
- [18] W. Lai, H. Wang, L. Zheng, Q. Jiang, Z.-C. Yan, L. Wang, H. Yoshikawa, D. Matsumura, Q. Sun, Y. Wang, Q. Gu, J.-Z. Wang, H.-K. Liu, S. Chou, and S.-X. Dou, *Angewandte Chem. Inte. Edition* **59**, 22171 (2020).
- [19] L. Zhao, Y. Zhang, L.-B. Huang, X.-Z. Liu, Q.-H. Zhang, C. He, Z.-Y. Wu, L.-J. Zhang, J. Wu, W. Yang, L. Gu, J.-S. Hu, and L.-J. Wan, *Nat. Commun.* **10**, 1278 (2019).
- [20] H. Fei, J. Dong, Y. Feng, C. S. Allen, C. Wan, B. Voloskiy, M. Li, Z. Zhao, Y. Wang, H. Sun, P. An, W. Chen, Z. Guo, C. Lee, D. Chen, I. Shakir, M. Liu, T. Hu, Y. Li, A. I. Kirkland, X. Duan, and Y. Huang, *Nat. Catalysis* **1**, 63 (2018).
- [21] G. Kresse and J. Hafner, *Phys. Rev. B* **47**, 558 (1993).
- [22] G. Kresse and J. Furthmüller, *Phys. Rev. B* **54**, 11169 (1996).
- [23] J. P. Perdew, K. Burke, and M. Ernzerhof, *Phys. Rev. Lett.* **77**, 3865 (1996).
- [24] P. E. Blöchl, *Phys. Rev. B* **50**, 17953 (1994).
- [25] A. Togo and I. Tanaka, *Scr. Mater.* **108**, 1 (2015).
- [26] G. J. Martyna, M. L. Klein, and M. Tuckerman, *J. Chem. Phys.* **97**, 2635 (1992).
- [27] See Supplemental Material at <http://link.aps.org/supplemental/10.1103/PhysRevB.103.125407> for the crystal structures of  $\text{CoN}_4\text{C}_{10}$ ,  $\text{Co}_2\text{N}_8\text{C}_6$ , and  $\text{Co}_2\text{N}_6\text{C}_6$  in the format of cif file.
- [28] Y. Sun, Z. Zhuo, X. Wu, and J. Yang, *Nano Lett.* **17**, 2771 (2017).
- [29] C. Ataca, M. Topsakal, E. Aktürk, and S. Ciraci, *J. Phys. Chem. C* **115**, 16354 (2011).
- [30] G. Henkelman, A. Arnaldsson, and H. Jónsson, *Comput. Mater. Sci.* **36**, 354 (2006).
- [31] Y. Cao, V. Fatemi, S. Fang, K. Watanabe, T. Taniguchi, E. Kaxiras, and P. Jarillo-Herrero, *Nature (London)* **556**, 43 (2018).
- [32] M. Yankowitz, S. Chen, H. Polshyn, Y. Zhang, K. Watanabe, T. Taniguchi, D. Graf, A. F. Young, and C. R. Dean, *Science* **363**, 1059 (2019).